

pubs.acs.org/JPCB Article

## Influence of Charge Regulation and Charge Heterogeneity on Complexation between Polyelectrolytes and Proteins

Published as part of The Journal of Physical Chemistry virtual special issue "Peter J. Rossky Festschrift". Rituparna Samanta, Avni Halabe, and Venkat Ganesan\*



Cite This: J. Phys. Chem. B 2020, 124, 4421–4435



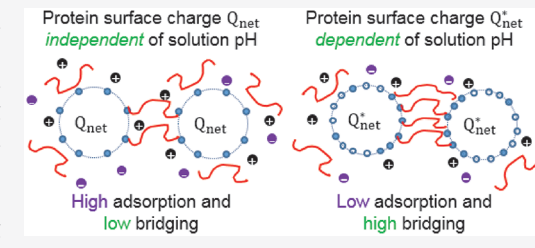
ACCESS

III Metrics & More



Supporting Information

**ABSTRACT:** We employed a combination of single chain in mean field methodology and constant pH Monte Carlo framework to compare the influence of charge regulation and charge heterogeneity on the adsorption and bridging characteristics of polyelectrolytes in solution on proteins. By adopting a coarse-grained representation of the proteins as spherical particles and embedding a simple framework for probing charge heterogeneities, we probe the influence of charge patches, net charge of the particle, the ratio of positive to negative charges on the proteins on the net adsorption, and bridging probabilities of polyelectrolytes. Our results demonstrate that charge regulation



increases the probability of bridging between two particles when compared to proteins with the same fixed charge. The influence of charge regulation first increases and then decreases with an increase in the number of charge patches of proteins. An increase in the ratio of positive to negative charges and the net charge of the protein are also seen to increase the propensity for polyelectrolyte adsorption and bridging.

#### 1. INTRODUCTION

Mixtures of proteins and polyelectrolytes (PE) are widely used in food systems to modulate the structure, texture, and stability of food through the resulting thickening and gelling characteristics. <sup>1–5</sup> Furthermore, PEs are often used to stabilize enzymes in biosensors <sup>6,7</sup> and in applications such as drug delivery by microencapsulating proteins, <sup>8</sup> design and production of biomaterials for cell micropatterning, <sup>9</sup> and selective extraction of proteins. <sup>10–13</sup> Mixtures of globular proteins and PEs also share a number of similarities to charged nanoparticle (NP)-PE systems. The complexes and assemblies resulting in the latter systems are important in applications such as optoelectronics, <sup>14–16</sup> microimaging, sensing, and so on. <sup>17,18</sup>

Many of the above-mentioned applications rely on the formation of a phase denoted as coacervate or complex which typically arises when there is an attractive interaction between the protein and the PE. In such phases, the electrostatic repulsion arising between the proteins is countered by the adsorption and bridging by the PEs. There have been a number of experimental studies aimed at understanding the physics underlying the structural characteristics, phase behavior, and complexation in protein-PE mixtures. 1,3,19 Such studies have demonstrated that the resulting phase behavior can be influenced by a variety of factors, which includes the physical characteristics of proteins and PEs, such as the charge distribution, geometry, and architecture, in addition to other parameters such as solution conditions and temperature. Due to the vast parameter space, there have also been a significant number of simulation studies which have probed the influence of different parameters on the complex formation of proteins in PE solutions.  $^{20-26}$ 

In a series of experiments, Dubin and co-workers have shown that the pH and the ionic strength of the solution exerts a strong influence on the complex formation between proteins and PEs. 19,27,28 A particularly intriguing result from their work (and other experiments from different groups)5,27,29 is the demonstration that such complexes can even form in solution pH conditions at which the charge of the protein is of the same sign as that of the PE. This latter phenomenon is termed "wrong side complexation", 12,19,27,28,30 and has been commonly rationalized through two distinct explanations: (i) charge heterogeneities on proteins and (ii) charge regulation. The first explanation invokes the existence of heterogeneous pockets of opposite charges on the protein, termed charge patches. It has been hypothesized that such patches allow the PEs to adsorb to the oppositely charged regions of the protein despite the protein being overall of the same charge as the PE. 31-33 The second explanation, viz., charge regulation, 34,35 relies on the dissociation characteristics of the charges on proteins in the presence of PEs. Indeed, similar to conventional

 Received:
 March 6, 2020

 Revised:
 April 30, 2020

 Published:
 May 26, 2020





acids and bases, dissociation of the charges on the proteins can be influenced by solution pH and the relative difference of the  $pK_a$  (or  $pK_b$ ) of the protein from pH. Such dissociation can further be influenced by the presence of PEs. The explanation of charge regulation relies on PE-induced charges in dissociation characteristics in promoting the adsorption, bridging, and complexation between PEs and proteins.

Despite the vast number of theoretical studies examining the influence of charge heterogeneity and charge regulation on the interactions between PEs and proteins, <sup>24,32,33,35–37</sup> much of the earlier work addresses the physics underlying such phenomena individually, <sup>24,37</sup> and typically for specific protein characteristics. 32,35 In this study, we take the first step toward understanding more generally the relative roles of charge regulation and charge patches on the complexation of PEs and proteins. To render such a generalization, we use a simple representation of spherical particles to represent globular proteins. To acknowledge the simplicity of our model, hereafter, we refer to the proteins interchangeably as charged particles. Within such a representation, we embed a "toy" model for probing the effect of charge heterogeneities. Using such a framework, we compare and contrast the effect of charge regulation and charge patches on adsorption and bridging of PEs on proteins. We report the results for adsorption and bridging characteristics for one and two particles in a multiple PE solution. While complexation typically involves multiple proteins, we believe that the insights resulting from the systematic study of one- and two-particle characteristics, especially the PE bridging in the two-particle case, could prove useful to understand the complexation behavior for systems involving multiple proteins in PE solution. Within such a context, we focus on design variables such as concentration of the PEs, net charge of the proteins, charge distribution on the proteins, and elucidate their influence on the adsorption and bridging characteristics of the PEs.

The rest of the article is organized as follows: In section 2, we discuss the details of the model underlying the simulation methodology used in this study. In section 3, we discuss the parameters and numerical methodologies used for the simulation framework. In section 4, we present the results of the study. Therein, we compare the influences of charge regulation and charge heterogenieties on the adsorption and bridging of PEs. We conclude the article with a summary of results and findings in section 5.

#### 2. MODEL DESCRIPTION

In this work, we focus on globular proteins and adopt a simple model of (charged) spherical particles to model such entities. Real proteins are likely to embody physics in which the positive, negative, and neutral charge patches are distributed in a manner which correlates with the underlying sequence and the solution conditions. Toward studying the effect of such patches, in our previous publication, we proposed a simple "toy" model in which the charge heterogeneities were represented as clusters of oppositely charge patches distributed on the surface of the particle. The "number of patches" denote the number of regions on which there are positive charges (shown in Figure 1). The sum of the charges of all such positive patches is denoted as  $Q_{\rm p}$ , and that of negative patches is denoted as  $Q_{\rm n}$ . The net charge of the protein is  $Q_{\rm net} = Q_{\rm p} - Q_{\rm n}$ . In our terminology, "PIN" denotes a patchy particle with N negatively charged patches, with PIO representing the case of

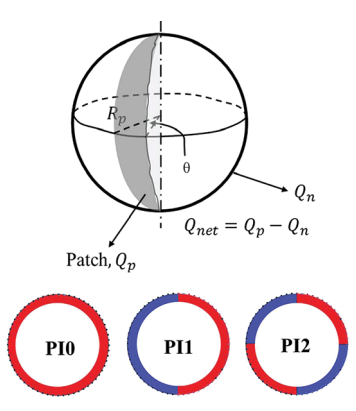


**Figure 1.** Model for patchy particles. The red color shows patches of positive charge, and the blue color depicts negative patches. The net charge of the positive patch is denoted as  $Q_{\rm p}$  and the net charge of the negative patch is denoted as  $Q_{\rm n}$ .

an homogeneous positively charged particle. In this article, we focus our discussion only on the results for "PIO", "PI1", "PI2", and "PI3" particles which contains zero, one, two, and three negative patches, respectively. For this study, the positive patches were assumed to be a weak base and consist of dissociable groups which can dissociate to a unity positive charge depending on the solution pH. For simplicity, we assume the negative patches of the particle to be a strong acid, such that the charge on the patch is fixed and independent of the solution pH.

We consider a system of heterogeneously charged spherical particles of radius  $R_{\rm p}$  and n negatively charged polymer chains of m monomers each in a periodic cubic box of volume V. We chose m=120 for this study. To maintain the overall electroneutrality of the system,  $n_{\rm p}$  and  $n_{\rm m}$  point counterions for the particles and polymers, respectively, are also included. To maintain simplicity, in this work, we did not consider the influence of additional salt. Hereafter, the concentration of the polymer is described in units of the overlap concentration  $C^*$  of an ideal linear polymer chain solution. The charge on each of the monomers of the polymer is  $z_{\rm m}=-1$ . We assume the dielectric constant of the particle to be same as that of the solvent. For the amphoteric particles, dissociation of the positive patch depends on pOH - p $K_{\rm b}$ .

We assume a flexible chain model for the PEs, in which the intramolecular interactions in the polymer chains are modeled through a bead spring model, with bonded Hookean interactions between the beads:

$$\frac{H_{\rm b}}{k_{\rm B}T} = \frac{3}{2b^2} \sum_{i=1}^{n} \sum_{s=1}^{m-1} \left[ \mathbf{r}_i(s) - \mathbf{r}_i(s+1) \right]^2$$
 (1)

where  $\mathbf{r}_i(s)$  represents the coordinate of the *s*th bead on the *i*th polymer. b is the bond length between two monomers. Excluded volume interactions between the polymer segments are incorporated through a simple implicit solvent interaction potential of the form:

$$\frac{\overline{u}(\mathbf{r})}{k_{\rm B}T} = u_0 \delta(\mathbf{r}) \tag{2}$$

where  $u_0$  is commonly known as the excluded volume parameter.<sup>39</sup> In the above framework, the nonbonded interactions between the polymer segments can be formally recast as

$$\frac{H_{\rm s}}{k_{\rm B}T} = \frac{u_0}{2} \int \hat{\rho}_{\rm poly}^2(\mathbf{r}) \, \mathrm{d}\mathbf{r} \tag{3}$$

where  $\hat{
ho}_{\text{poly}}$  is the microscopic polymer segment density  $^{40}$ 

$$\hat{\rho}_{\text{poly}}(\mathbf{r}) = \sum_{i=1}^{n} \sum_{s=1}^{m} \delta[\mathbf{r} - \mathbf{r}_{i}(s)]$$
(4)

The instantaneous density of particles is similarly quantified through a particle volume fraction field as

$$\rho_{\text{part}}(\mathbf{r}) = \sum_{i=1}^{N_{\text{p}}} \int_{r_i}^{r_i + R_{\text{p}}} \hat{\rho}_{\text{part}}(\mathbf{r}) h(|\mathbf{r}' - \mathbf{r}_i|) d\mathbf{r}'$$
(5)

where  $\hat{\rho}_{part}(\mathbf{r}) = \delta(\mathbf{r} - \mathbf{r}_i)$  and h(r) = 1 when  $|r| < R_p$ . The counterions are considered to be point charges and their microscopic densities are given by

$$\rho_{\text{mi}}(\mathbf{r}) = \sum_{i=1}^{n_{\text{m}}} \delta(\mathbf{r} - \mathbf{r}_i)$$

$$\rho_{pi}(\mathbf{r}) = \sum_{i=1}^{n_p} \delta(\mathbf{r} - \mathbf{r}_i)$$
(6)

For modeling particle—counterion and particle—monomer interactions, the particles are envisioned as spherical objects with a thin layer of penetrable soft core surrounding an impenetrable hard core. The repulsive interaction between the particle and the polymer monomers, counterions are modeled through an interaction potential of the form:

$$W_{\rm cp}(\mathbf{r}) = 50 \left[ 1 - \tanh \left( 2 \frac{\mathbf{r} - \alpha R_{\rm p}}{\beta} \right) \right] k_{\rm B} T \tag{7}$$

The coefficients  $\alpha$  and  $\beta$  control the steepness and range over which the repulsive potential decays from  $100k_{\rm B}T$  to  $0k_{\rm B}T$ . We have used  $\alpha=0.9$  and  $\beta=0.5$  nm for the simulation, which ensures that the particle cores are almost impenetrable to counterions and polymers. The direct interparticle interactions are modeled through a hard-sphere interaction:

$$\frac{H_{\rm pp}}{k_{\rm B}T} = \frac{1}{2} \sum_{i=1}^{N_{\rm p}} \sum_{j=1(j\neq i)}^{N_{\rm p}} U_{\rm HS}(|\mathbf{r}_i - \mathbf{r}_j|)$$
(8)

where

$$U_{\text{HS}}(r) = \begin{cases} 0 & \text{if } r \ge 2R_{\text{p}} \\ \infty & \text{if } r < 2R_{\text{p}} \end{cases}$$
(9)

For the simulations of the structure of polyelectrolyte–protein mixtures, we have used the single chain in mean field (SCMF) approach introduced by Mueller and co-workers. <sup>22,23,41–43</sup> The SCMF simulation is an approximate method that retains the advantage of self-consistent field theory (SCFT) in addition to the fluctuation effects. In this particle-based simulation, independent chains are evolved in an external field; these external fields are the instantaneous interaction of molecules surrounding and their densities. These instantaneous fields and densities are discretized in space. The positions of particles are updated using Monte Carlo (MC) analysis based on these quasi-instantaneous fields. The accuracy of SCMF is dependent on the frequency at which the fields are updated (enough to mimic the instantaneous fields) and discretization of space and chain length. <sup>41,44</sup> The

statistical segments of the Gaussian chain in our system interact through the excluded volume parameter (to capture the effect of solvent),  $u_0$ , while the charge segments interact via a Coulombic interaction which depends on the Bjerrum length and the charge space on the polymer backbone, which is determined by b. In our system, the presence of each species is used to calculate the density and potential fields with a spatial collocation mesh of resolution of  $\Delta x = 0.7b$ . We performed the simulations in a periodic cubic box of length  $L \approx 37b$ , which was sufficient to minimize finite size effects. We note that our model framework assumes that the monomers and counterions are point particles. Thereby, in this paper we are not considering several factors including short-range potentials like hard-core interactions and ion size effects. 45,46 For instance, Li et al. studied the effect of ion size on charge distribution of counter- and co-ions near a charged surface by minimizing a free energy functional using the Poisson's equation as the constraint. With a decrease in size of the counterion, the saturation value of counterion concentration far away from the charged surface increased, and the width of the saturation region was found to decrease.<sup>45</sup> Such effects are not captured within the SCMF approach.

In the SCMF framework, the nonbonded pairwise interactions are replaced with fluctuating potential fields which are conjugate to the corresponding density fields. The electrostatic energy arising from the charges is represented in terms of its conjugate electrostatic potential field  $\varphi(\mathbf{r})$  and the associated energy:

$$\frac{H_{\rm el}}{k_{\rm B}T} = \int d\mathbf{r} \left[ \rho_{\rm e}(\mathbf{r}) \varphi(\mathbf{r}) - \frac{1}{8\pi l_{\rm b}} |\nabla \varphi(\mathbf{r})|^2 \right]$$
(10)

where  $\rho_{\rm e}({\bf r})$  is the total charge density arising from particles, polymers, and counterions (in units of e), and is given as

$$\rho_{\rm e}(\mathbf{r}) = z_{\rm part}(\mathbf{r}) \, \rho_{\rm part}(\mathbf{r}) \, \pm \, \sum_{\rm ion} z_{\rm ion} \, \rho_{\rm ion}(\mathbf{r}) \, - \, z_{\rm m} \, \hat{\rho}_{\rm poly}(\mathbf{r})$$
(11)

where  $z_{\rm ion}$  is the valency of each ion (co- or counterions),  $z_{\rm m}$  is the valency of each monomer,  $z_{\rm part}({\bf r})$  is the local charge of the particle which in turn depends on the sign and magnitude of the particle patch at  ${\bf r}$ . Field  $\rho_{\rm ion}({\bf r})$  denotes the local density of co- and counterions. The electrostatic potential  $\varphi({\bf r})$ , in units of  $k_{\rm R}T/e$ , is obtained as the solution of Poisson's equation:

$$\nabla^2 \varphi(\mathbf{r}) = -4\pi l_b \rho_e(\mathbf{r}) \tag{12}$$

In the above equation,  $l_{\rm b}$  is the Bjerrum length, defined as  $e^2/4\pi\varepsilon_0\varepsilon_{\rm r}k_{\rm B}T$ , where  $\varepsilon_{\rm r}$  is the relative dielectric constant of the medium and  $\varepsilon_0$  is the vacuum permittivity. For water, at 300 K,  $l_{\rm b}\approx 0.7$  nm.

To accommodate the dissociation of particles within the above simulation method we have embedded the constant pH simulation method within the existing SCMF framework (depicted schematically in Figure 2a,b). <sup>47,48</sup> The "constant pH" algorithm relies on the global pH/pOH value as an input to modulate the probability of association and dissociation of the dissociable species. An association/dissociation reaction of a titratable group on the surface (on the positive patch) of an annealed protein can be written as

$$BOH \leftrightarrow B^+ + OH^{-1}$$

where BOH denotes the associated form of the titratable group, B<sup>+</sup> is the dissociated form and OH<sup>-1</sup> is the hydroxyl ion.

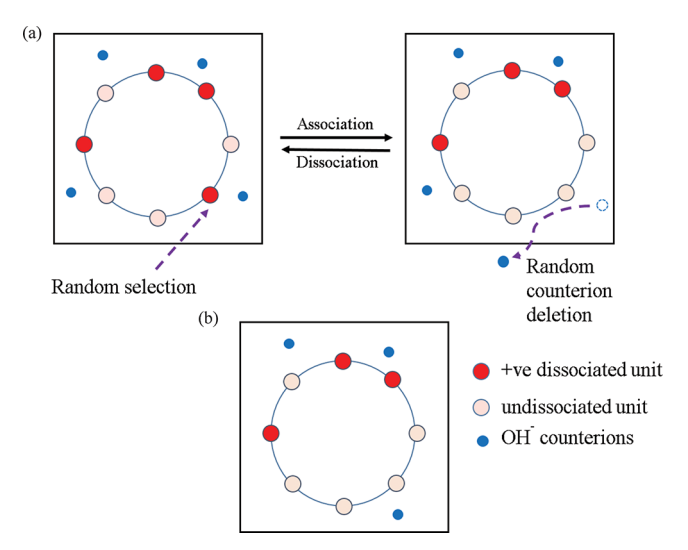


Figure 2. Schematic depiction of the computational method which is a hybrid of a constant pH method and SCMF, pertaining to an annealed PIO particle. (a) A dissociable unit is chosen at random. It can be changed from a dissociated state to an undissociated and vice versa based on a metropolis condition. On the basis of the dissociation state, a counterion is deleted from or added to the system. (b) On the basis of the charge of the protein and the number of counterions in the system after step (a), SCMF is performed on the counterions, PEs, and the particles in a canonical system. The above steps are then repeated multiple times (details in section 3) to attain equilibrium properties.

The probability of dissociation or association is determined after two steps. First, a random titratable group is chosen in the simulation box, either a BOH or a B<sup>+</sup>. It can be changed from a dissociated state to an undissociated state and vice versa based on a Metropolis criterion. The trial move for reaction is accepted with a probability given as

$$\operatorname{acc}(\operatorname{association}) = \min \left[ 1, \frac{N_{\text{BOH}}}{N_{\text{H}^+}} 10^{(\text{pOH}_{\text{in}} - \text{pK}_{\text{B}})} \exp^{-\Delta E_{\text{pot}}} \right]$$

$$\operatorname{acc}(\operatorname{dissociation}) = \min \left[ 1, \frac{N_{\text{B}^+}}{N_{\text{BOH}}} 10^{-(\text{pOH}_{\text{in}} - \text{pK}_{\text{B}})} \exp^{-\Delta E_{\text{pot}}} \right]$$

$$(13)$$

where  $\Delta E_{pot}$  is the potential energy change due to the change in characteristics of each species. Here  $\Delta E_{\rm pot}|_{\rm dissociation}=z_{\rm m}\varphi$ and  $\Delta E_{\rm pot}|_{\rm association} = -z_{\rm m}\varphi$ , where  $\varphi$  is the local electrostatic field. pOH<sub>in</sub> is the input pOH which determines the implicit pOH value of the solution. Another input to the simulation is  $pK_B$ , where  $K_B$  is the basicity constant. Second, if an undissociated unit is converted from it is uncharged state to a charged state, then a counterion is added. In contrast, if a dissociated unit is converted from its charged state to an uncharged state, then a counterion is deleted from the system. It is to be noted that the dissociation of each dissociable unit on the surface of the protein depends on the electrostatic potential based on their position, which in turn depends on the surrounding charge distribution. In our simulation we have ignored the possibility of autoprotolysis reaction of water  $(H_2O \leftrightarrow H^+ + OH^{-1})$ . In this work we have assumed electrostatic interaction to be dominant with respect to other interactions such as dipole-dipole or hydrogen bonding.

#### 3. NUMERICAL METHODS AND PARAMETERS

The model described in the previous section is used in a MC simulation approach in which the configuration space is sampled using the Metropolis algorithm. 49 For the case of single-particle simulations, we began by placing the particle at the center of the box and the PEs and the counterions in random positions in the rest of the box. In the initial portion of the simulation, 10<sup>4</sup> MC moves are performed such that only the PEs are moved while keeping the particles fixed in space. This pre-equilibrium is done to ensure removal of any particle-polymer overlaps. Subsequently, each MC step (MCS) involved a slithering snake move for all polymer chains and 100 MC moves for all monomers and counterions. To calculate the charge of the particle, a protonation/ deprotonation move (as seen in Figure 2a) is performed for all the dissociable components (of particles) once every 100 MC moves for the polymers. Using the position of the monomers and ions, the density fields, charge density fields, and electrostatic fields are updated after every move of the polymer and particles. Using such a sequence of moves, the system is equilibrated for  $5 \times 10^4$  MCS. Subsequently, the properties are averaged over 5 × 10<sup>4</sup> MCS, constituting the production cycle.

As a complement to the results for polymer density profiles and adsorption on a single particle, we also studied the polymer bridging characteristics for two particles. Since our study focuses only on one- and two-particle systems, we view the polymer bridging characteristics as a means to understand the propensity for complexation in protein—PE mixtures. For quantifying the bridging characteristics of PEs, the probability of bridging (will be discussed in detail in the subsequent paragraphs) is calculated by placing a second particle at a distance "r" from the center of the first particle. For such analyses, every MCS move also included a rotational move for the second particle to accommodate the relative orientation of the charge heterogenieties of the particles. After every such rotation, each monomer of the polymer present in the box is moved for 100 MC cycles (10<sup>4</sup> MC steps).

We use a Fast Fourier Transform (FFT) based numerical method to solve the Poisson's equation (eq 12).  $^{22,23,50-52}$  For our study, we have used the Bjerrum length ( $l_{\rm b}$ ) as 0.7 nm, corresponding to that of water at 300 K. Furthermore, we have kept the value of  $u_0$  = 10, representing a good solvent. We note that previous studies from our group have suggested that excluded volume interactions exert only a small influence on the results for good solvent conditions. The particles used in the simulation are of radii  $R_{\rm p}$  = 10 nm, and the homopolymers are of  $R_{\rm g}$  = 24 nm. For the simulation, we have used a periodic cubic box of size (200 nm)<sup>3</sup>  $\approx$  20 $R_{\rm p}$  × 20 $R_{\rm p}$  × 20 $R_{\rm p}$  divided into a 64 × 64 × 64 grid. In this study, we did not probe the effect of varying  $R_{\rm p}$  or  $R_{\rm g}$ . Unless otherwise noted, the concentration of polymer in the system is set at  $C/C^*$  = 0.10.

We characterize the PE adsorption on the particles by the measure net adsorption (eq 15):

Net adsorption = 
$$\int_{R_p}^{\infty} d^3 \mathbf{r} (\rho_{\text{pol}}(\mathbf{r}) - \rho_{\text{avg}})$$
 (15)

where  $\rho_{\rm pol}({\bf r})$  and  $\rho_{\rm avg}$  denote the local and bulk polymer concentrations, respectively. To characterize the PE bridging characteristics, we set out to quantify the probability that a

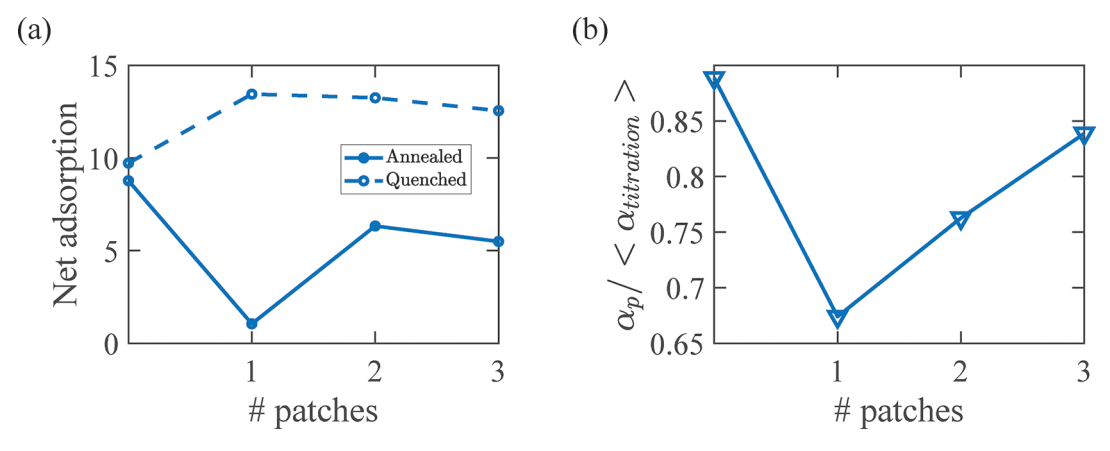


Figure 3. (a) Net adsorption of polymers on annealed and quenched particles. (b) Ratio of dissociation of the annealed particles in a PE solution to that in the PE-free solution.

particle is connected to the other by at least one polymer bridge:

$$P_{\rm f}(r) = \frac{\text{No. config. at which at least 1 polymer bridges between 2 particles}}{\text{Total no. config.}}$$

As discussed previously, the calculation of bridging characteristics involve rotational moves for a fixed center to center distance "r" between two particles. Such calculations are comparatively expensive and as a consequence are statistically less reliable due to the number of configurations that could be sampled. To obtain qualitative insights into the influence of different parameters on bridging characteristics,  $P_t(r)$  is fit to a function of the following form shown in eq 17:  $^{53,54}$ 

$$P_{\rm f}(r) = c \times \left(1 - \tanh\left(\frac{r - a}{b}\right)\right) \tag{17}$$

where *a*, *b*, and *c* are the fitting parameters. We use the resulting fits to discuss the influence of different physical parameters with bridging characteristics. The raw data and the corresponding fits are shown in Figure S1a—d.

### 4. RESULTS AND DISCUSSION

To elucidate the influence of charge regulation on PE adsorption and bridging characteristics, we compare the results of the dissociable particle model with that of the case in which the patchiness of the particles are retained, but the charge themselves are fixed. In accord with the terminology commonly used in this regard, the dissociable particles are termed "annealed" particles, whereas the fixed charge model is termed a "quenched" particle. S1,S5,S6 To ensure a valid comparison between such systems for each pH probed, we chose the number of dissociable units for the annealed particles such that the net charge of the annealed particles in (a PE-free) solution at the specified pH matches with that of the quenched particles.

In the following, we discuss the combined influence of charge patchiness and charge regulation on PE adsorption and bridging characteristics. Subsequently, we present results elucidating the influence of other variables such as the charge of patches, the net charge of the particle and the polymer concentration on adsorption and bridging characteristics.

**4.1. Effect of Number of Patches on the Protein.** In this section, we discuss the effect of the number of patches on

the protein on the adsorption and bridging characteristics. We compare and contrast the results for quenched and annealed particles.

Figure 3a presents results comparing the net adsorption (eq 15) of PEs on annealed and quenched particles. The quenched particles are assumed to possess the same net charge  $Q_{\rm net} = 14$  while possessing different charge distributions corresponding to PI0, PI1, PI2, and PI3 (detailed charge distribution data are shown in Table 1). The patchy particles, which have both

Table 1. Detailed Charge Distribution of Patchy Proteins

		quenched		annealed	
type	no. of negative patch	$Q_{p}$	Qn	$Q_p$	$Q_{\rm n}$
PI0	0	$(Q_{\rm net})$	0.0	$Q_{\text{net}}/\alpha_{\text{titration}} = 40.0$	0.0
PI1	1	38.0	24.0	84.0	24.0
PI2	2	38.0	24.0	95.0	24.0
PI3	3	38.0	24.0	110.0	24.0

positive and negative patches, are chosen such that all the models have the same  $Q_p$  and  $Q_n$ . As seen from the results in Figure 3a, the net adsorption of PEs on the quenched particles is higher than that on the annealed ones, suggesting that charge regulation leads to a reduction in polymer adsorption. For quenched cases, we observe that the net adsorption of PEs on patchy particle to be higher than homogeneous particles. However, for annealed particles, the net adsorption is seen to first decrease and then increase with the number of patches.

Prior to rationalization of the above results, we note that the net adsorption of PEs on patchy particles involves a competition between the adsorption of PEs on the opposite charged patches and the electrostatic (and entropically) induced depletion of PEs from the negatively charged patches. The former is dependent on the charge density of the positive patch, while the latter depends on the charge density of the negative patch. Within such a context, the above differences in the adsorption characteristics behavior can be explained using two-dimensional representation of the resulting PE concentrations (Figure 4a—h) for the different systems.

To explain the influence of charge heterogeneities on the adsorption characteristics of quenched patchy particles, we observe from Figure 4a—d that the concentration of the polymer near the positive patch for PI1 is higher than that for PI0. This arises as a consequence of the higher charge of the

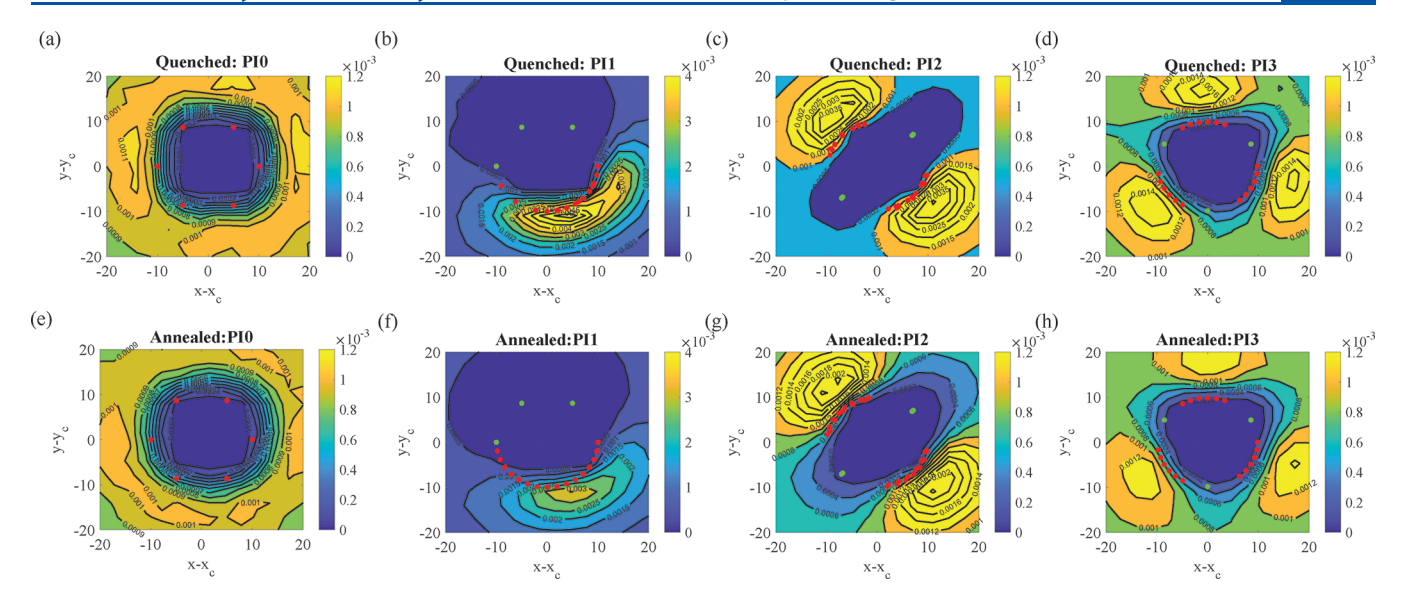


**Figure 4.** (a-d) Local concentration of PEs around annealed patchy particles. (e-h) Local concentration of PEs around quenched patchy particles. The red dots denote the positively charged dissociable units, and the green dots present the negatively charged units on the proteins. ( $x_c$ ,  $y_c$ ) are the (x, y) coordinates of the center of the first particle. The key to the color map is shown in the color bars.

positively charged patch in PI1 particles relative to the PI0 particles (note that the  $Q_{\rm net}$  is maintained the same between PI0, PI1, PI2, and PI3 particles). As a result, there is an increase in the net adsorption for PI1 particles compared to PI0 particles. With an increase in the number of patches, the concentration of polymers near the positive patches decreases, since the local charge of each positive patch decreases. In addition, the repulsion from the negative patches and the accompanying polymer depletion increases due to their proximity to the positive charge patches. Together, these effects lead to a reduction in the net adsorption for quenched particles with larger number of patches.

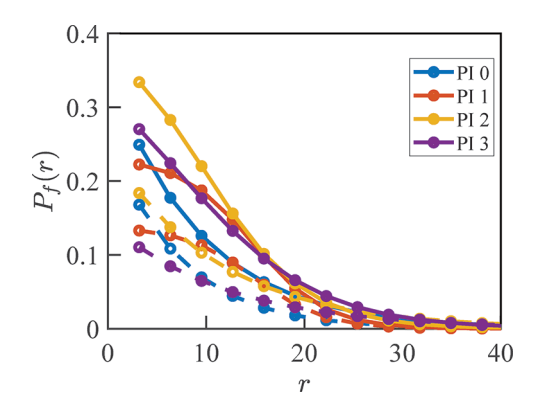
For annealed particles (Figure 3a), the concentration distribution of polymers follows a trend similar to that for quenched particles. However, for annealed patchy particles, the concentration of PEs near the positive patch is seen to be lower than that of the quenched particles. To explain these differences, in Figure 3b we display the resulting dissociation of annealed particles in the presence of PEs relative to that in PE-free solution. For all cases, this ratio is seen to be less than 1.0, which indicates that the net positive charge of the annealed particles in the presence of PEs is lower than that of the quenched particles. The latter result can be understood by noting that the dissociation of annealed particles depend on the local density of the oppositely charged entities. In the presence of negatively charged PEs in the solution, positively charged counterions are also introduced to ensure electroneutrality in the system. The presence of positive counterions reduces the dissociation of the positive patch of the particles to mitigate unfavorable electrostatic interactions. A similar result was presented in Pryamitsyn et al. in the context of adsorption of PEs on oppositely charged particles (at higher concentration

Using the above results, we can rationalize the lower net adsorption of polymers in annealed particles as arising from the lower charges of such particles in the presence of PEs. Further support of the above reasoning is seen in the fact that the decrease and the increase in the net adsorption (Figure 3a) of patchy particles relative to the homogeneous particles correlate

well with the relative ratio of the degree of dissociation seen in Figure 3b.

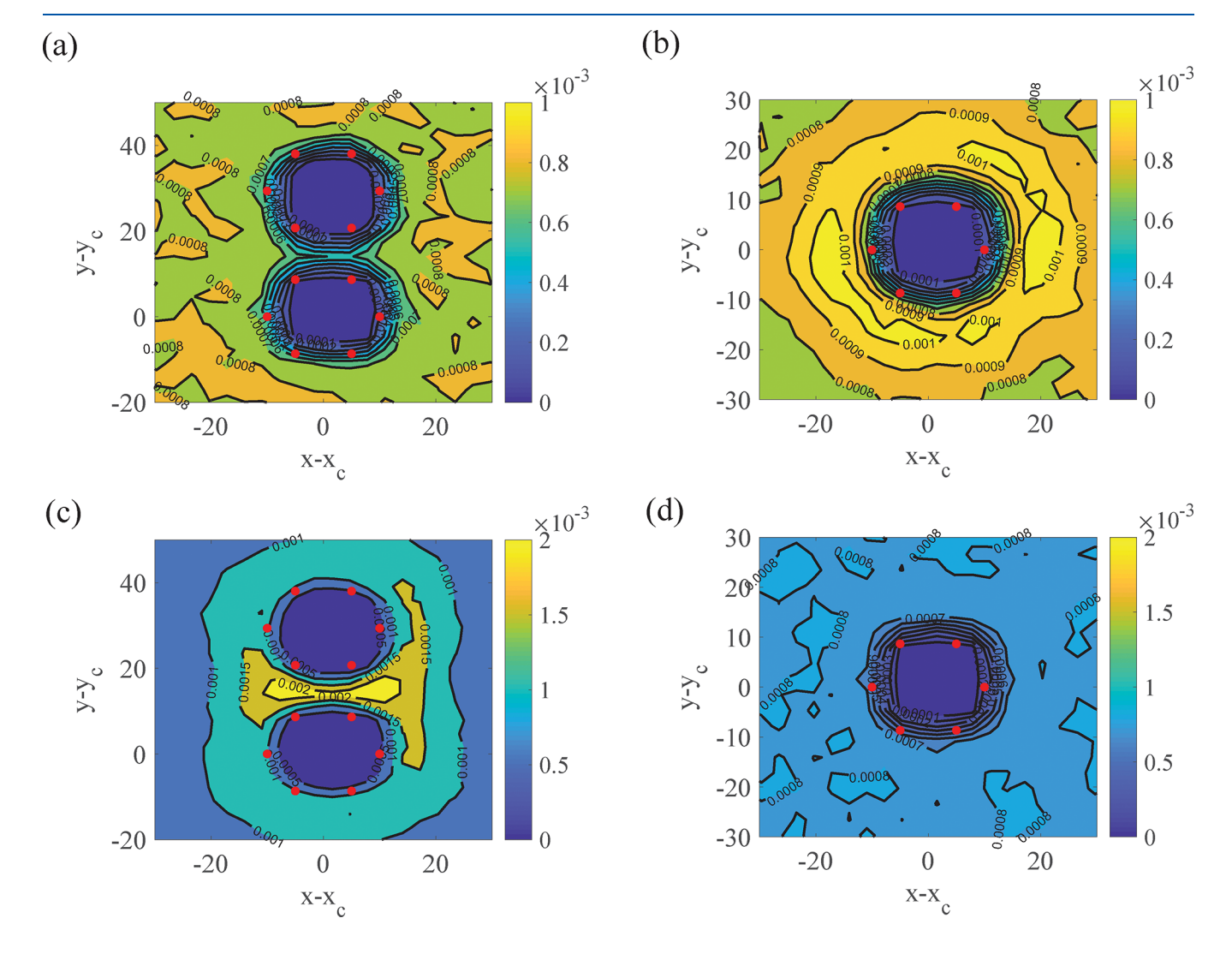
The influence of the number of patches on the dissociation and net adsorption for the annealed particles can be explained by using the two-dimensional PE concentrations in Figure 4eh. Similar to the reasoning presented for quenched particles, for patchy particles (PI1, PI2, and PI3), the concentration of negatively charged polymers is seen to be higher than that of the homogeneously charged PIO particles due to the lower positive charge density of the latter. However, in the case of annealed particles, an increase in concentration of the negatively charged polymers also increases the local concentration of positively charged counterions. Such a higher density of counterions near the particle causes the dissociation of the positive patch to decrease for PI1. When the number of patches increases, the concentration of the polymers near the positive patch reduces due to both the decreased charge of each positive patch and the increased proximity of the negative patches. This reduction in polymer concentration leads to a lowering of the concentration of positive counterions near the positive patches. The latter leads to an increase in the dissociation of PI2 and PI3 particles relative to PI1 particles. Hence, the adsorption for annealed particles first decreases and then increases with the increase in the number of patches.

Figure 5 presents results for the probability of bridge formation,  $P_{\rm f}(r)$ , comparing the quenched and annealed particles. Surprisingly, in contrast to the results for polymer adsorption, it can be seen that the probability of bridging is higher for all annealed particles (solid lines) than for the corresponding quenched ones (dashed lines). The trends for quenched particles are seen to follow the behavior for PE adsorption, such that the probability of bridging for patchy particles is slightly higher than that for the homogeneous particles. For annealed particles, when compared to PIO particles, the probability of bridging (at a given distance) decreases for PII. However, compared to PII, and similar to the trend observed for adsorption,  $P_{\rm f}(r)$  first increases and then decreases with further increases in patchiness.



**Figure 5.** Probability of bridging,  $P_{\hat{p}}$  for patchy particles as a function of surface to surface distance r for different number of patches on the particle. The dashed lines corresponds to quenched particles, and the solid lines present the results for the annealed particles.

To rationalize the above results, in Figure 6a,b we present the concentration of positive counterions for annealed PIO particles in a two-particle system and compare it with that in a single-particle system. It can be seen that relative to a singleparticle system the local concentration of positive counterions is lowered and the polymer concentration becomes enhanced with the introduction of the second particle. To demonstrate that similar effects manifest for patchy particles, we present the results corresponding to PI1 particles fixed in three configurations. The three representative configurations displayed are as follows: (a) Positives: corresponding to the case where the two positive faces are opposite to each other. (b) Negatives: corresponding to the case where the two negative faces are opposite to each other. (c) Opposites: corresponding to the case where the two oppositely charged faces are opposite to each other (Figure 7b-d). In the displayed results, it is seen that the counterion concentration for the two-particle system is again lower near the positive patch (relative to that of the oneparticle system as seen in Figure 7a). Thus, such results demonstrate that the presence of the second particle and the electrostatic interactions arising from the latter leads to a reduction in the counterion concentration near the positive patches of the annealed particles.



**Figure 6.** Local concentration of positive counterions around PIO annealed particles in a two-particle system, (b) single-particle system. The polymer density around PIO annealed particles corresponding to (c) the two-particle system and (d) the one-particle system. The red dots denote the positively charged dissociable units on the proteins.  $(x_c, y_c)$  are the (x, y) coordinates of the center of the first particle. The key to the color map is shown in the color bars.

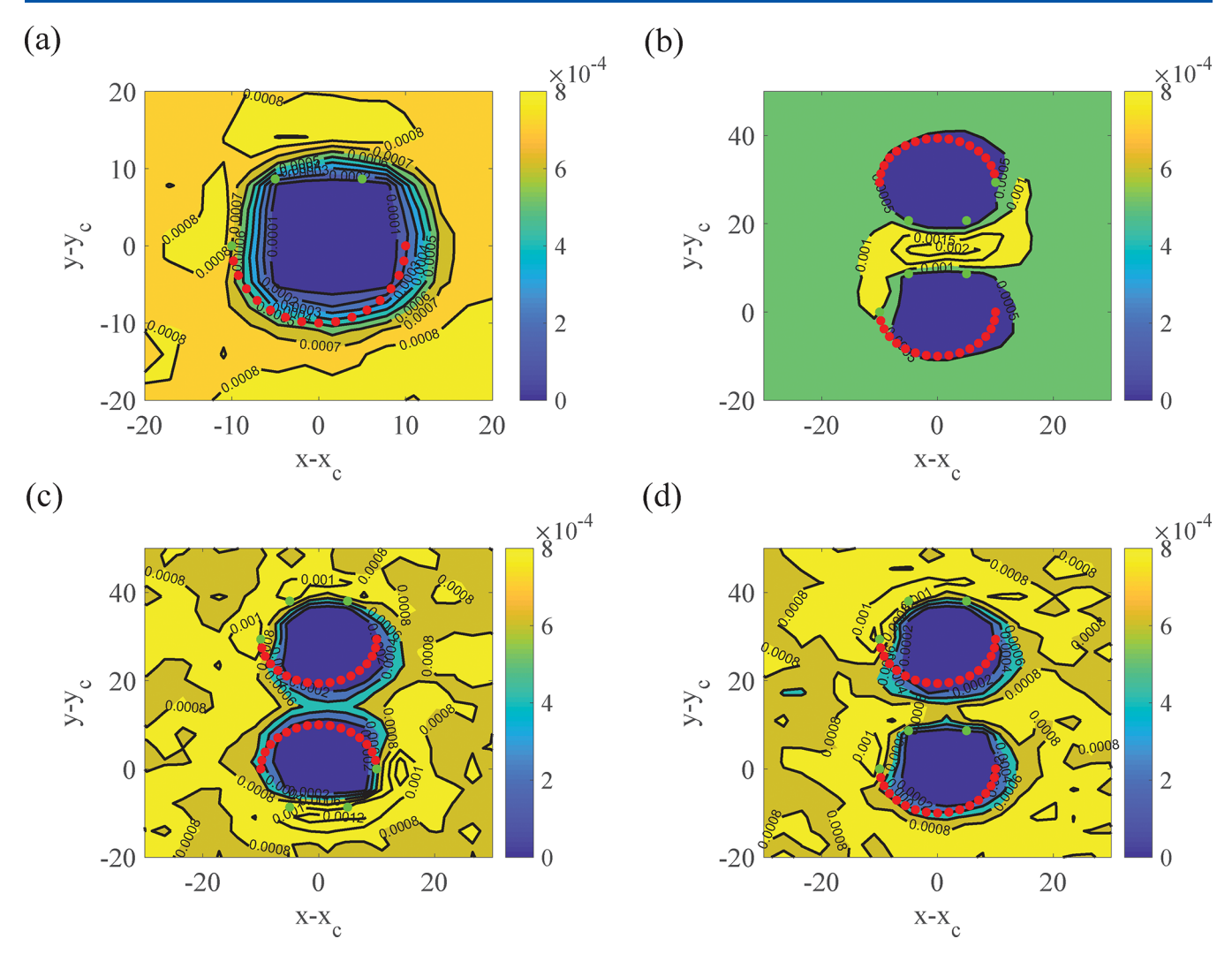


Figure 7. (a) Local concentration of positive counterions around an annealed PI1 particle. Local concentrations of positive counterion around two annealed PI1 particles fixed with their (b) negative patches facing each other, (c) positive patches facing each other, and (d) opposite patches facing each other. The red dots denote the positively charged dissociable units and the green dots denote the negatively charged units on the proteins. ( $x_c$ ,  $y_c$ ) are the (x, y) coordinates of the center of the first particle. The key to the color map is shown in the color bars.

We suggest that the above-discussed lower concentration of positive counterions in the two-particle system is the origin of the enhanced bridging seen for annealed particles. Indeed, the reduction in counterion concentration is expected to enhance the dissociation of charged entities on the positive patch of the annealed particles. Such an expectation is confirmed in the results presented in Figure 8a—c which displays the local charge distributions for the annealed particles. Such an enhanced dissociation is expected to increase the electrostatic attraction between the PE and the particle and leads to a concomitant increase in the PE adsorption and bridging for the annealed particles (Figure 9a) relative to the quenched particles (Figure 9c).

To summarize the results of this section, for single particles, the net PE adsorption on quenched particles was seen to be higher than that on annealed particles. This was argued to arise as a consequence of the reduction in the net charge of the positive patch in the presence of oppositely charged polyelectrolytes. However, in contrast to such results, the probability of bridge formation was seen to be higher for annealed particles when compared to quenched particles. The latter results were shown to arise due to the influence of the

second particle on the charge dissociation of the annealed particles. Such charge regulation effects are seen to be enhanced further by the presence of charge patches. On the basis of such results, we conclude that charge regulation serves to be an important factor in regulating polymer bridging of charged particles. Moreover, while the influence of charge regulations is enhanced through the presence of charge heterogeneities, such effects are seen to be only at a secondary level. While our results pertain to only two-particle systems, if we hypothesize that similar considerations carry over to multiple particle systems, then the presence of dissociable charges and the accompanying charge regulation is likely to enhance complexation above and beyond what may be expected based on the charge of the particle in PE-free solution.

# **4.2.** Effect of Charges on the Patches of the Proteins. To probe further the influence of charge heterogeneities on the adsorption and bridging characteristics, we adopted a framework in which we changed the ratio of positive to negative patch charge $(Q_p/Q_n)$ while keeping the net charge of the particle $(Q_{\rm net} = Q_p - Q_n)$ constant. Such a framework was inspired by protein supercharging experiments, <sup>57,58</sup> where the

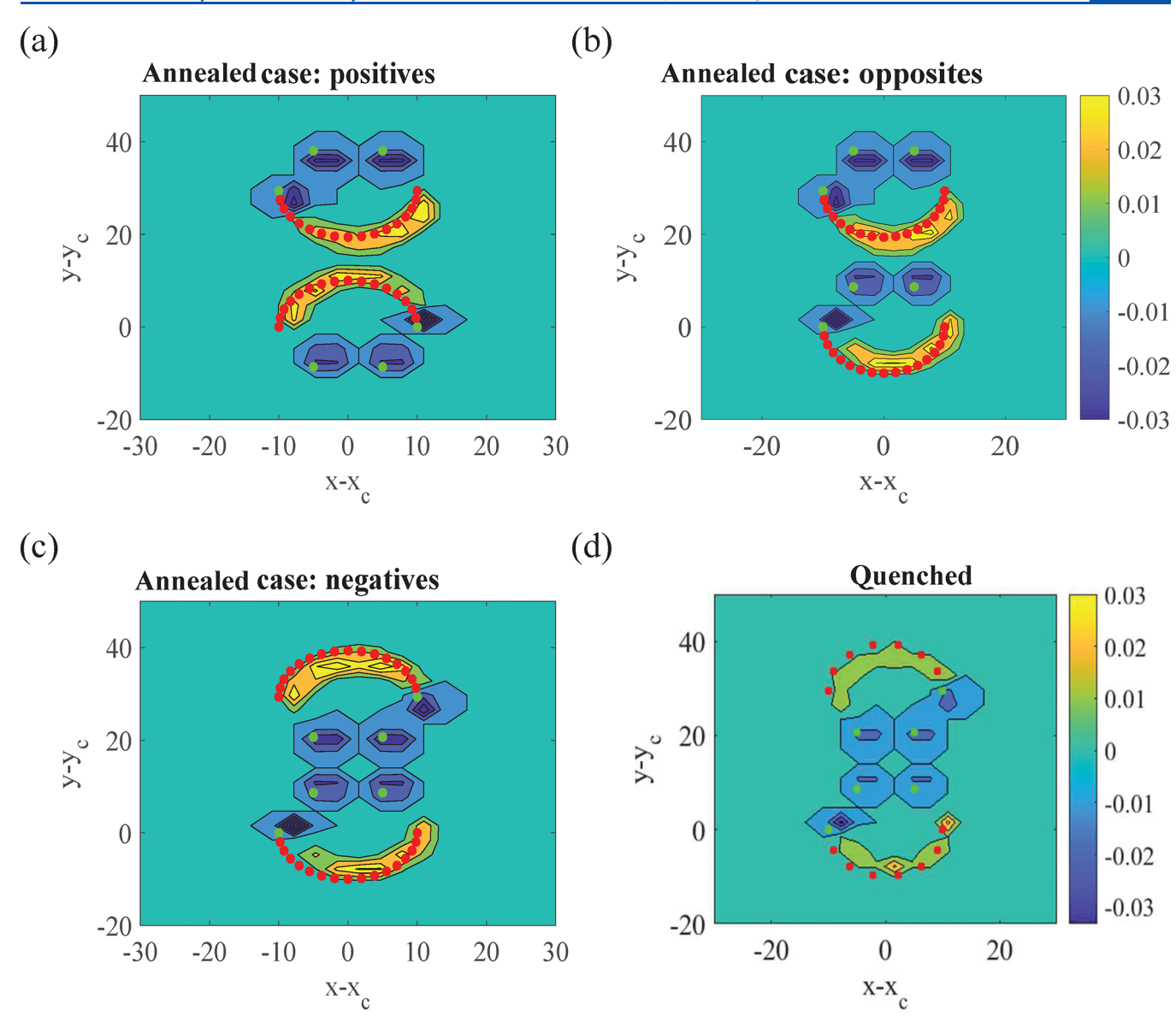


**Figure 8.** Average charge of annealed PI1 particles with their (a) positive patches facing each other, (b) oppositely charged patches facing each other, (c) negatively charged patches facing each other, (d) quenched PI1 particles. The red dots denote the positively charged dissociable units. The green dots denote the negatively charged units.  $(x_0, y_0)$  are the  $(x_0, y_0)$  coordinates of the center of the first particle.

net charge of the protein can be either increased or decreased by manipulating the surface charges of specific regimes.

Figure 10a,b presents the result for adsorption for PI1 particles with fixed  $Q_{net} = 14$  with different ratio between the positive and negative patches. From the results in Figure 10a, we observe that the adsorption for quenched particles initially increases with an increase in the charge of the positive patch and then beyond a critical charge decreases with further increase in the positive charge. The initial increase in net adsorption can be rationalized as arising from the increased electrostatic interaction between the positive patch and PEs. However, since our framework for this keeps the net charge fixed, this increase in positive charge is also accompanied by an increase in the charge on the negative patches, which concomitantly leads to an increase in the repulsive interactions between the PEs and the negatively patches. Due to such competing factors, the net adsorption of polymers first increases and then decreases with increase in the charge of the positive patch of the particle.

In Figure 10a, the net adsorption of the *annealed* particles is seen to decrease with an increase in the charge of the positive patch of the particle. In line with the results presented in the previous section, this decrease in net adsorption is seen to be consistent with the decrease in the degree of dissociation of the positive patch with an increase in  $Q_p$  (in Figure 10b). The latter can in turn be explained as arising from the higher concentration of positive ions near the positive patches as seen in the Figure S2a-c. The increase in the concentration of counterions near the positive patch is due to the higher local concentration of negatively charged PEs with increase in the charge of the positive patch of the particle.

Figure 11 presents a comparison of the results for  $P_{\rm f}(r)$  between PI1 quenched and annealed particles with constant  $Q_{\rm net}=14$  but different charges on patches. Similar to the results seen in the previous section, annealed particles are seen to exhibit a higher probability of bridge formation than that for quenched particles. To maintain brevity, we do not repeat the earlier discussed physics underlying such results which relates

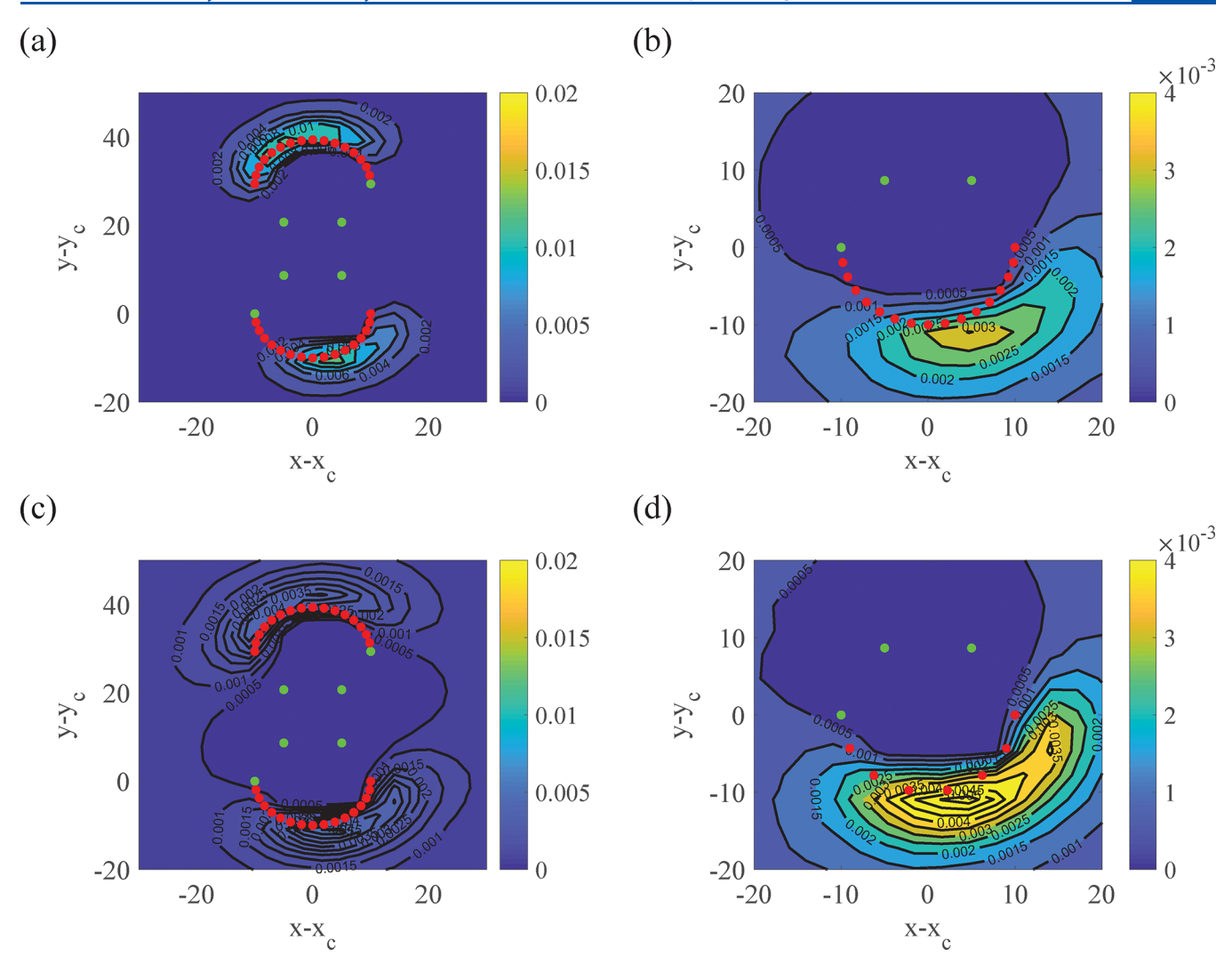


**Figure 9.** Local concentrations of polymers (a) around two annealed PI1 particles at a fixed position with their negative patches facing each other, (b) for a single PI1 annealed particle, (c) for two quenched PI1 particles at a fixed position with their negative patches facing each other, and (d) for a single PI1 quenched particle. The red dots denote the positively charged dissociable units. The green dots denote the negatively charged units.  $(x_o, y_c)$  are the (x, y) coordinates of the center of the first particle. The key to the color map is shown in the color bar.

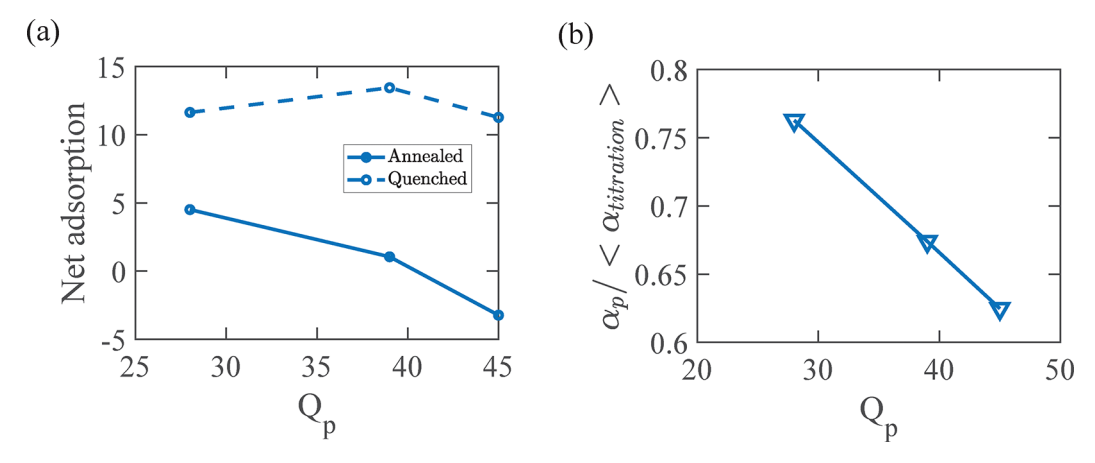
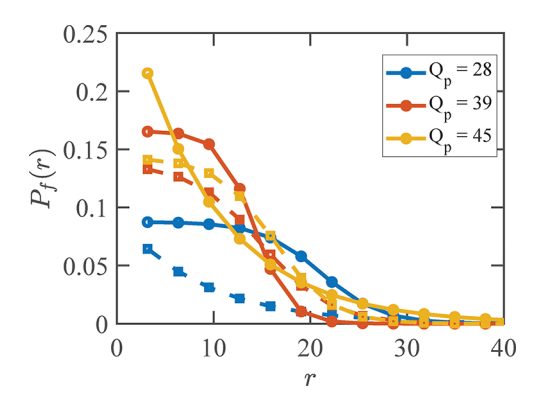


Figure 10. (a) Net adsorption of polymers on annealed and quenched particles. (b) The ratio of dissociation constant of the annealed particles in the presence of PEs compared to that in a PE-free solution.

to the local dissociation of the charge patches and the density of counterions arising in the presence of the second particle.

With regards to the influence of the charge on the positive patch, the  $P_{\rm f}(r)$  for the quenched particles is seen to initially

increase with an increase in charge of the positive patch. This increase can be rationalized by the increase in electrostatic attraction (between the oppositely charged PE and the positive patch) with an increase in charge of the positive patch and



**Figure 11.** Probability of bridging,  $P_{\theta}$  as a function of surface to surface distance between the particles r for different charges of the positive patch,  $Q_{\rm p}$ . The dashed lines present results for quenched patchy particles. The solid lines present results for the annealed patchy particles.

correlates with the results for the polymer adsorption as seen in Figure 10a. Relative to  $Q_{\rm p}=39$ , the probability of bridging increases only by a small amount for  $Q_{\rm p}=45$  due to the increased electrostatic repulsion arising from the negative patch of the particle which reduces polymer adsorption.

For the annealed particles, the probability of bridging is also seen to increase with an increase in the charge of the positive patch (Figure 11). Similar to the results discussed in section 4.1, for all values of  $Q_p$ , the counterion concentrations near the positive patches are lower for the annealed two-particle system when compared to those for the one-particle system (as seen in Figure S3). Furthermore, the differences in the concentration of counterions near the positive patch between the one- and two-particle systems increases with an increase in  $Q_p$  (seen in Figure S3a-f). This increased depletion of the positive counterions can be rationalized as arising from the increase in the electrostatic repulsion from the positive patches of the second particle. This decrease in concentration of counterions leads to an increase in dissociation of the positive patch and a corresponding increase in polymer adsorption and bridging.

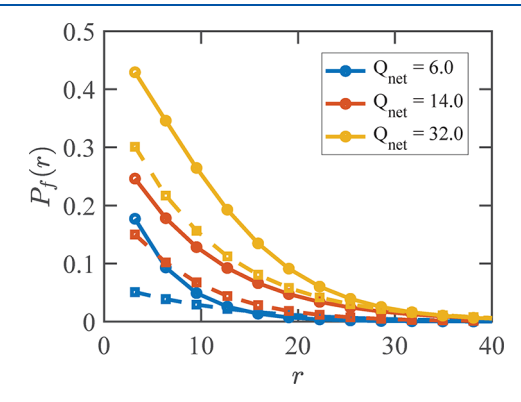
**4.3.** Effect of the Net Charge of the Proteins. To probe the influence of net charge of the proteins on the adsorption and bridging, here we consider only the case of homogeneously charged particles, PIO. Similar to the previous sections, we adopted a framework where the net charge of the quenched particle is kept the same as that of the average charge of the

annealed particle after dissociation in PE-free solution. Such a framework ensures that the difference in adsorption or bridging behavior arises only due to charge regulation.

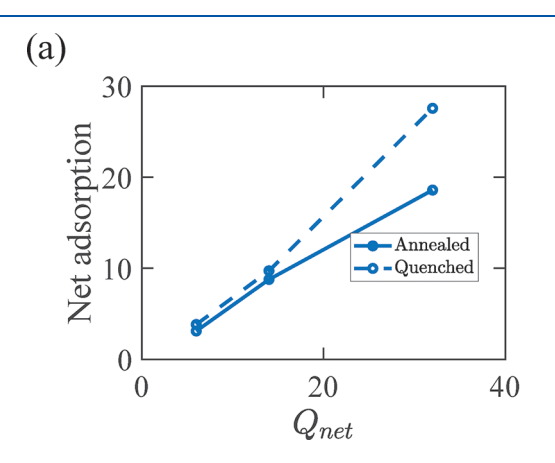
Figure 12a,b presents the results of adsorption of PEs on annealed and quenched particles for different net charges. From the results presented in Figure 12a, we observe that the adsorption for both quenched and annealed particles increases with increase in the net charge of the particle. Such an observation is intuitive and can be rationalized by the increase in the electrostatic attraction between the PEs and the particles with increase in particle charges.

The net adsorption for annealed particles is observed to be lower than that of the quenched particles for all charges. Moreover, the difference between the net adsorption of quenched and annealed particles is seen to increase with an increase in their net charge. Such observations can be again rationalized by invoking the extent of dissociation (as seen in Figure 12b) of the annealed particles in the presence of PEs. Explicitly, in Figure 12b the dissociation of particles in the presence of PEs is seen to be lower than that in PE-free solution, and decreases with an increase in the net charge of the particles. This reduction in dissociation can be rationalized due to increase in the concentration of positive counterions near the particles, an effect similar to that observed by Pryamitsyn et al.<sup>50</sup>

Figure 13 presents the results for  $P_f(r)$  for quenched and annealed particles for different net charges.  $P_f(r)$  is seen to



**Figure 13.** Probability of bridging,  $P_{\rm fi}$  as a function of particle surface to surface distance r for different  $Q_{\rm net}$ . The dashed lines corresponds to quenched particles. The solid lines correspond to annealed particles.



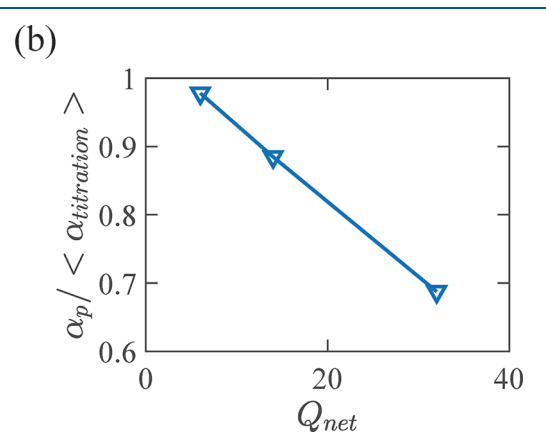


Figure 12. (a) Net adsorption of polymers on annealed and quenched particles. (b) The ratio of dissociation constant of the particles in the presence of PEs compared to that in the PE-free solution.

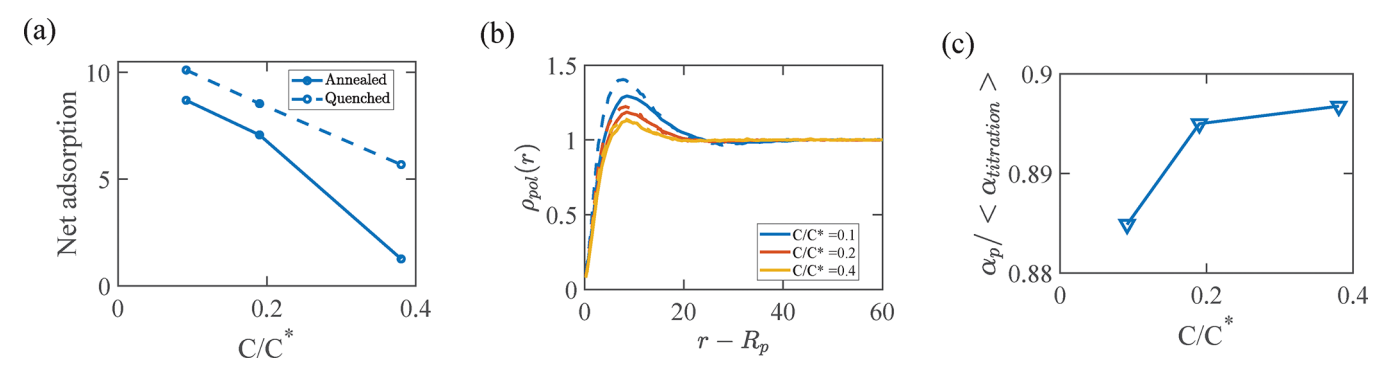


Figure 14. (a) Net adsorption of polymers on annealed and quenched particles. (b) Local polymer concentrations (normalized) around a particle. (c) Ratio of dissociation constant of annealed particles in the presence of PEs compared to that in PE-free solution.

increase with increase in the net charge of the particles for both annealed and quenched particles. This trend can be rationalized by invoking the enhancement in electrostatic attraction between the particle and polymer resulting at higher particle charges.  $P_{\rm f}(r)$  for annealed particles is again seen to be higher than that for the quenched particles. Similar to the results discussed in previous sections, the counterion concentrations for the two-particle system is reduced relative to that for the one-particle system (seen in Figure S5a-f) leading to an increase in polymer adsorption (as seen in Figure S6a-f) and bridging due to increase in dissociation (as seen in Figure S7a).

With regards to the influence of  $Q_{\rm net}$  on the bridging of annealed particles, in Figure S5a-f, it can be seen that the differences in counterion concentration between the two- and one-particle systems increases with an increase in  $Q_{\rm net}$  particularly in the area between two particles. This can be rationalized as arising from the increased electrostatic repulsions experienced by the positive counterions due to the second particle. Such a depletion of counterions causes an enhanced dissociation of the particles and an increase in the concentration of polymers (Figure S6a-f). This results in the differences between  $P_{\rm f}(r)$  of quenched and annealed particles to increase with an increase in  $Q_{\rm net}$ .

**4.4. Effect of Polymer Concentration.** To probe the effect of polymer concentration on the adsorption on quenched and annealed particles, in this section we maintain the net charge of PIO at  $Q_{\rm net}=14$  and vary the polymer concentration.

The results presented in Figure 14a demonstrate that with an increase in concentration of the polymers the net adsorption for both annealed and quenched particles decreases. To rationalize such an observation, we present the local concentration of polymers normalized by the bulk concentration as seen in Figure 14b in which the polymer concentration profile is seen to have a peak followed by a long-range decay. It is further observed that the peak of the polymer concentration decreases with an increase in the bulk concentration of the polymer. This reduction in the peak of the concentration and the range of concentration is responsible for the reduction in the net adsorption.

The above results are similar to those presented in Pryamitsyn et al.,<sup>51</sup> where the peak in the polymer concentration was rationalized by suggesting that at dilute polymer concentrations, the local polymer concentrations were enhanced (relative to bulk) to neutralize the charge on the particle. In contrast to higher bulk polymer concentrations, the local polymer concentrations were suggested to reflect

neutralization of counterions segregated to the particle surface and are hence comparable to the bulk concentration of the polymers. Furthermore, the reduction in the range of the concentration variation was argued to arise as a consequence of increased electrostatic screening.

The net adsorption for annealed particles are seen to be slightly lower than quenched particles and follow the same trends with respect to the polymer concentration. Similar to the results discussed in the previous sections, the differences between annealed and quenched particles can be rationalized by invoking the dissociation for the particle and its value relative to a PE-free solution (shown in Figure 14c), which is seen to increase very slightly with the concentration of polymers. This latter observation is in line with the results shown by Pryamitsyn et al. at low bulk PE concentration sand can be understood by noting that an increase in the bulk concentration of the polymer leads to an increase in the dissociation of the particles to accommodate favorable electrostatic interaction between the particles and the oppositely charged polymers.

Figure 15 presents results comparing  $P_f(r)$  in quenched and annealed particles for different concentration of polymers. As

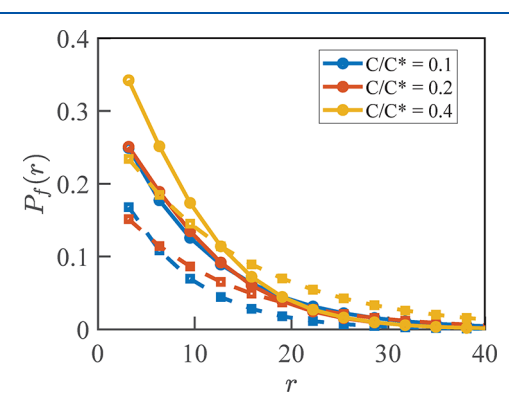


**Figure 15.** Probability of bridging,  $P_{\theta}$  as a function of particle surface to surface distance r for different  $C/C^*$ . The dashed lines correspond to quenched particles. The solid lines correspond to annealed particles.

may be expected intuitively,  $P_{\rm f}(r)$  is seen to increase with an increase in the bulk concentration of the polymers. Similar to the results in the previous sections, the  $P_{\rm f}(r)$  for quenched particles is again seen to be lower than the annealed particles, and the difference between them decreases with an increase in concentration of the polymer.

To rationalize the influence of polymer concentration on the differences between  $P_f(r)$  for annealed and quenched particles, Figure S8a-f presents results comparing the average counterion concentration around annealed particles. In line with the results discussed in the previous section, the average counterion concentration around the annealed particles are seen to be lower relative to that in an one-particle system (as seen in Figure S8) resulting in a higher dissociation of particles, enhanced polymer adsorption, and bridging. With an increase in the concentration of polymers, there is expected to be an increase in the electrostatic screening and therefore diminished role for the differences in counterion concentrations to influence the dissociation of annealed particles. This leads to reduction in the difference between  $P_{\rm f}(r)$  for annealed and quenched particles with increase in the concentration of the polymer.

#### 5. CONCLUSIONS

In the previous section, we have presented results for the influence of different charge distribution on the particles, net charge of the particles, and concentration of the PEs on the adsorption and bridging of PEs on the particles. For all cases, quenched particles, i.e., for situations in which the net charge of the particle was fixed, the net adsorption of polymer was seen to be higher than that of the annealed particles. Such results were rationalized as arising from the reduction in dissociation of annealed particles in the presence of PEs relative to a PE-free solution. The differences between the net adsorption in quenched vs annealed particles were seen to increase with increase in the net charge of the particle, decrease in the number of patches and increase in the magnitude of the positive patches.

In contrast to results for net adsorption, the probability of bridging  $P_{\rm f}(r)$  was seen to be higher for the annealed particles when compared to that for the quenched particles. Such results were shown to occur due to increased dissociation of individual particles in the presence of the second particle. The charge regulation effect on bridging is enhanced by the presence of charge heterogeneity, increases in the charge of positive patch of the particles, and decreases with the concentration of the PEs.

The results presented in this study comprise a first step toward understanding the influence of charge regulation and charge heterogeneity on adsorption and bridging of PEs on proteins. Our results suggest that charge regulation can serve as a significant influence of polymer bridging and possibly PE complexation. In a future study, we plan to extend the framework of the present study to account for the influences of multiple particles and characterize the resulting structure and phase behavior in such cases.

#### ■ ASSOCIATED CONTENT

#### Supporting Information

The Supporting Information is available free of charge at https://pubs.acs.org/doi/10.1021/acs.jpcb.0c02007.

Raw data of  $P_{\rm f}(r)$  and its curve fitting, local positive counterion and polymer concentration around single and two-particle systems supporting the discussions in section 4.2–4.4, and plots of dissociation of PIO particles for one- and two-particle systems with the variation of  $Q_{\rm net}$  and  $C/C^*$  (PDF)

#### AUTHOR INFORMATION

#### **Corresponding Author**

Venkat Ganesan — Department of Chemical Engineering, University of Texas at Austin, Austin, Texas 78712, United States; orcid.org/0000-0003-3899-5843; Email: venkat@che.utexas.edu

#### **Authors**

Rituparna Samanta — Department of Chemical Engineering, University of Texas at Austin, Austin, Texas 78712, United States

Avni Halabe — Department of Chemical Engineering, University of Texas at Austin, Austin, Texas 78712, United States

Complete contact information is available at: https://pubs.acs.org/10.1021/acs.jpcb.0c02007

#### Notes

The authors declare no competing financial interest.

#### ACKNOWLEDGMENTS

The National Science Foundation (Grants DMR-1721512) and the Robert A. Welch Foundation (Grants F-1599) both supported this work. The results in this paper were generated using high-performance computing resources provided by The University of Texas at Austin Texas Advanced Computing Center.

#### REFERENCES

- (1) Schmitt, C.; Turgeon, S. L. Protein/polysaccharide complexes and coacervates in food systems. *Adv. Colloid Interface Sci.* **2011**, *167*, 63–70.
- (2) Comert, F.; Malanowski, A. J.; Azarikia, F.; Dubin, P. L. Coacervation and precipitation in polysaccharide-protein systems. *Soft Matter* **2016**, *12*, 4154–4161.
- (3) de Kruif, C. G.; Weinbreck, F.; de Vries, R. Complex coacervation of proteins and anionic polysaccharides. *Curr. Opin. Colloid Interface Sci.* **2004**, *9*, 340–349.
- (4) Tuinier, R.; Rieger, J.; de Kruif, C. Depletion-induced phase separation in colloid and polymer mixtures. *Adv. Colloid Interface Sci.* **2003**, *103*, 1–31.
- (5) Cummings, C. S.; Obermeyer, A. C. Phase separation behavior of supercharged proteins and polyelectrolytes. *Biochemistry* **2018**, *57*, 314–323.
- (6) Dumitriu, S.; Chornet, E. Inclusion and release of proteins from polysaccharide-based polyion complexes. *Adv. Drug Delivery Rev.* 1998, 31, 223–246.
- (7) Kim, B.; Lam, C. N.; Olsen, B. D. Nanopatterned protein films directed by ionic complexation with water-soluble diblock copolymers. *Macromolecules* **2012**, *45*, 4572–4580.
- (8) Armstrong, J. P. K.; Olof, S. N.; Jakimowicz, M. D.; Hollander, A. P.; Mann, S.; Davis, S. A.; Miles, M. J.; Patil, A. J.; Perriman, A. W. Cell paintballing using optically targeted coacervate microdroplets. *Chemical Science* **2015**, *6*, 6106–6111.
- (9) Shaikh Mohammed, J.; DeCoster, M. A.; McShane, M. J. Micropatterning of nanoengineered surfaces to study neuronal cell attachment in vitro. *Biomacromolecules* **2004**, *5*, 1745–1755.
- (10) Dubin, P. L.; Gao, J.; Mattison, K. Protein purification by selective phase separation with polyelectrolytes. *Sep. Purif. Methods* **1994**, 23, 1–16.
- (11) Wang, Y.; Gao, J. Y.; Dubin, P. L. Protein separation via polyelectrolyte coacervation: selectivity and efficiency. *Biotechnol. Prog.* **1996**, *12*, 356–362.
- (12) Xu, Y.; Mazzawi, M.; Chen, K.; Sun, L.; Dubin, P. L. Protein purification by polyelectrolyte coacervation: influence of protein charge anisotropy on selectivity. *Biomacromolecules* **2011**, *12*, 1512–1522.

- (13) Xu, Y.; Liu, M.; Faisal, M.; Si, Y.; Guo, Y. Selective protein complexation and coacervation by polyelectrolytes. *Adv. Colloid Interface Sci.* **2017**, 239, 158–167.
- (14) Maier, S. A.; Kik, P. G.; Atwater, H. A.; Meltzer, S.; Harel, E.; Koel, B. E.; Requicha, A. A. Local detection of electromagnetic energy transport below the diffraction limit in metal nanoparticle plasmon waveguides. *Nat. Mater.* **2003**, *2*, 229.
- (15) Nizri, G.; Makarsky, A.; Magdassi, S.; Talmon, Y. Nanostructures formed by self-assembly of negatively charged polymer and cationic surfactants. *Langmuir* **2009**, *25*, 1980–1985.
- (16) Yatsui, T.; Ryu, Y.; Morishima, T.; Nomura, W.; Kawazoe, T.; Yonezawa, T.; Washizu, M.; Fujita, H.; Ohtsu, M. Self-assembly method of linearly aligning ZnO quantum dots for a nanophotonic signal transmission device. *Appl. Phys. Lett.* **2010**, *96*, 133106.
- (17) Shi, L.; Carn, F.; Boue, F.; Mosser, G.; Buhler, E. Control over the electrostatic self-assembly of nanoparticle semiflexible biopolyelectrolyte complexes. *Soft Matter* **2013**, *9*, 5004–5015.
- (18) Thunemann, A. F. Polyelectrolyte-surfactant complexes (synthesis, structure and materials aspects. *Prog. Polym. Sci.* **2002**, 27, 1473–1572.
- (19) Cooper, C.; Dubin, P.; Kayitmazer, A.; Turksen, S. Polyelectrolyte-protein complexes. *Curr. Opin. Colloid Interface Sci.* **2005**, *10*, 52–78.
- (20) Russel, W. B.; Saville, D. A.; Schowalter, W. R. Colloidal Dispersions; Cambridge University Press, 1989; Vol. 54; pp 201–202.
- (21) Carlsson, F.; Linse, P.; Malmsten, M. Monte Carlo simulations of polyelectrolyte and protein complexation. *J. Phys. Chem. B* **2001**, 105, 9040–9049.
- (22) Pandav, G.; Pryamitsyn, V.; Ganesan, V. Interactions and aggregation of charged nanoparticles in uncharged polymer solutions. *Langmuir* **2015**, *31*, 12328–12338.
- (23) Pandav, G.; Pryamitsyn, V.; Errington, J.; Ganesan, V. Multibody interactions, phase behavior, and clustering in nanoparticle-polyelectrolyte mixtures. *J. Phys. Chem. B* **2015**, *119*, 14536–14550.
- (24) Ulrich, S.; Seijo, M.; Carnal, F.; Stoll, S. Formation of complexes between nanoparticles and weak polyampholyte chains. Monte Carlo Simulations. *Macromolecules* **2011**, *44*, 1661.
- (25) Ulrich, S.; Seijo, M.; Laguecir, A.; Stoll, S. Nanoparticle adsorption on a weak polyelectrolyte. Stiffness, pH, charge mobility, and ionic concentration effects investigated by Monte Carlo simulations. *J. Phys. Chem. B* **2006**, *110*, 20954–20964.
- (26) Ulrich, S.; Laguecir, A.; Stoll, S. Complexation of a weak polyelectrolyte with a charged nanoparticle. Solution properties and polyelectrolyte stiffness influences. *Macromolecules* **2005**, *38*, 8939–8949.
- (27) Park, J. M.; Muhoberac, B. B.; Dubin, P. L.; Xia, J. Effects of protein charge heterogeneity in protein-polyelectrolyte complexation. *Macromolecules* **1992**, *25*, 290.
- (28) Mattison, K. W.; Brittain, I. J.; Dubin, P. L. Protein-polyelectrolyte phase boundaries. *Biotechnol. Prog.* **1995**, *11*, 632–637.
- (29) Harnsilawat, T.; Pongsawatmanit, R.; McClements, D. J. Influence of pH and ionic strength on formation and stability of emulsions containing oil droplets coated by  $\beta$ -Lactoglobulin & Alginate interfaces. *Biomacromolecules* **2006**, 7, 2052–2058.
- (30) Mattison, K. W.; Dubin, P. L.; Brittain, I. J. Complex formation between Bovine Serum Albumin and strong polyelectrolytes: effect of polymer charge density. *J. Phys. Chem. B* **1998**, *102*, 3830–3836.
- (31) Kayitmazer, B. A.; Quinn, B.; Kimura, K.; Ryan, G. L.; Tate, A. J.; Pink, D. A.; Dubin, P. L. Protein specificity of charged sequences in polyanions and Heparins. *Biomacromolecules* **2010**, *11*, 3325–3331.
- (32) de Vries, R.; Weinbreck, F.; de Kruif, C. G. Theory of polyelectrolyte adsorption on heterogeneously charged surfaces applied to soluble protein and polyelectrolyte complexes. *J. Chem. Phys.* **2003**, *118*, 4649–4659.
- (33) de Vries, R. Monte Carlo simulations of flexible polyanions complexing with whey proteins at their isoelectric point. *J. Chem. Phys.* **2004**, *120*, 3475–3481.

- (34) kirkwood, J. G.; Shumaker, J. B. Forces between protein molecules in solution arising from fluctuations in proton charge and configuration. *Proc. Natl. Acad. Sci. U. S. A.* **1952**, 38, 863–871.
- (35) Srivastava, D.; Santiso, E.; Gubbins, K.; Barroso da Silva, F. L. Computationally mapping pKa shifts due to the presence of a polyelectrolyte chain around Whey proteins. *Langmuir* **2017**, 33, 11417–11428.
- (36) da Silva, F. L. B.; Jonsson, B. Polyelectrolyte-protein complexation driven by charge regulation. *Soft Matter* **2009**, *5*, 2862–2868.
- (37) Stornes, M.; Shrestha, B.; Dias, R. S. pH-dependent polyelectrolyte bridging of charged nanoparticles. *J. Phys. Chem. B* **2018**, *122*, 10237–10246.
- (38) Samanta, R.; Ganesan, V. Influence of protein charge patches on the structure of protein polyelectrolyte complexes. *Soft Matter* **2018**, *14*, 9475–9488.
- (39) Doi, M.; Edwards, S. The Theory of Polymer Dynamics; Clarendon Press Publication, 1988.
- (40) Fredrickson, G. H. The Equilibrium Theory of Inhomogenous Polymers; Oxford Science Publications, 2006.
- (41) Daoulas, K. C.; Mueller, M. Single chain in mean field simulations: Quasi-instantaneous field approximation and quantitative comparison with Monte Carlo simulations. *J. Chem. Phys.* **2006**, *125*, 184904.
- (42) Detcheverry, F. A.; Kang, H.; Daoulas, K. C.; Mueller, M.; Nealey, P. F.; de Pablo, J. J. Monte Carlo simulations of a coarse grain model for block copolymers and nanocomposites. *Macromolecules* **2008**, *41*, 4989–5001.
- (43) Mueller, M.; Daoulas, K. C. Calculating the free energy of self-assembled structures by thermodynamic integration. *J. Chem. Phys.* **2008**, *128*, No. 024903.
- (44) Fredrickson, G. H.; Ganesan, V.; Drolet, F. Field-theoretic computer simulation methods for polymers and complex fluids. *Macromolecules* **2002**, *35*, 16–39.
- (45) Zhou, S.; Wang, Z.; Li, B. Mean-field description of ionic size effects with nonuniform ionic sizes: a numerical approach. *Phys. Rev. E* **2011**, *84*, No. 021901.
- (46) Sing, C. E.; Zwanikken, J. W.; de la Cruz, M. O. Theory of melt polyelectrolyte blends and block copolymers: phase behavior, surface tension, and microphase periodicity. *J. Chem. Phys.* **2015**, *142*, No. 034902.
- (47) Reed, C. E.; Reed, W. F. Monte Carlo study of titration of linear polyelectrolytes. *J. Chem. Phys.* **1992**, *96*, 1609–1669.
- (48) Mueller, M.; Smith, G. D. Phase separation in binary mixtures containing polymers: A quantitative comparison of single-chain-in-mean-field simulations and computer simulations of the corresponding multichain systems. *J. Polym. Sci., Part B: Polym. Phys.* **2005**, 43, 934–958.
- (49) Metropolis, N.; Rosenbluth, A. W.; Rosenbluth, M. N.; Teller, A. H.; Teller, E. Equation of State Calculations by Fast Computing Machines. *J. Chem. Phys.* **1953**, *21*, 1087–1092.
- (50) Pryamitsyn, V.; Ganesan, V. Pair interactions in polyelectrolytenanoparticle systems: influence of dielectric inhomogeneities and the partial dissociation of polymers and nanoparticles. *J. Chem. Phys.* **2015**, *143*, 164904.
- (51) Pryamitsyn, V.; Ganesan, V. Interplay between depletion and electrostatic interactions in polyelectrolyte and nanoparticle systems. *Macromolecules* **2014**, 47, 6095–6112.
- (52) Samanta, R.; Ganesan, V. Influence of dielectric inhomogeneities on the structure of charged nanoparticles in neutral polymer solutions. *Soft Matter* **2018**, *14*, 3748–3759.
- (53) Surve, M.; Pryamitsyn, V.; Ganesan, V. Nanoparticles in solutions of adsorbing polymers: pair interactions, percolation, and phase behavior. *Langmuir* **2006**, *22*, 969–981.
- (54) Surve, M.; Pryamitsyn, V.; Ganesan, V. Universality in structure and elasticity of polymer—nanoparticle gels. *Phys. Rev. Lett.* **2006**, *96*, 177805
- (55) Guo, X.; Ballauff, M. Spherical polyelectrolyte brushes: comparison between annealed and quenched brushes. *Phys. Rev. E:*

- Stat. Phys., Plasmas, Fluids, Relat. Interdiscip. Top. 2001, 64, No. 051406.
- (56) Biesheuvel, P. M.; Wittemann, A. A modified box model including charge regulation for protein adsorption in a spherical polyelectrolyte brush. *J. Phys. Chem. B* **2005**, *109*, 4209–4214.
- (57) Lawrence, M. S.; Phillips, K. J.; Liu, D. R. Supercharging proteins can impart unusual resilience. *J. Am. Chem. Soc.* **2007**, *129*, 10110–10112.
- (58) Obermeyer, A. C.; Mills, C. E.; Dong, X.-H.; Flores, R. J.; Olsen, B. D. Complex coacervation of supercharged proteins with polyelectrolytes. *Soft Matter* **2016**, *12*, 3570–3581.